Coarse-grained modelling of pressure-related effects in staphylococcal nuclease and ubiquitin

2007 J. Phys.: Condens. Matter 19 285218

(http://iopscience.iop.org/0953-8984/19/28/285218)

IOP PUBLISHING JOURNAL OF PHYSICS: CONDENSED MATTER

J. Phys.: Condens. Matter **19** (2007) 285218 (14pp) doi:10.1088/0953-8984/19/28/285218

Coarse-grained modelling of pressure-related effects in staphylococcal nuclease and ubiquitin

Michal Wojciechowski and Marek Cieplak

Institute of Physics, Polish Academy of Sciences, Aleja Lotników 32/46, 02-668 Warsaw, Poland

Received 6 April 2007, in final form 22 May 2007
Published 25 June 2007
Online at stacks.iop.org/JPhysCM/19/285218

Abstract

Folding and unfolding kinetics of proteins are affected by the application of high hydrostatic pressure. In order to study the pressure-related effects within geometry-based coarse-grained models, we propose adding a pressure-controlled hump to the contact potentials. This approach qualitatively reproduces the experimental findings on conformational changes in staphylococcal nuclease and predicts a non-monotonic dependence of the unfolding time with pressure. The pressure-induced unfolding is shown to be distinct from unfolding induced by a high temperature.

1. Introduction

Applying pressure to fluids with proteins is an interesting tool for probing the properties of proteins [1–6] that has been in use since the beginning of the twentieth century [7]. Pressure variations are relatively easy to implement. The effects that they cause are expected to be reversible, since they usually do not involve chemical reactions (a very high pressure could cause an aggregation of unfolded proteins that could be irreversible). Pressures of around 2–3 kbar can dissociate most oligomeric proteins without any significant changes in subunit conformations [8, 9], whereas pressures above 3–4 kbar begin to unfold monomeric proteins [10].

Due to instrumental limitations, studies of protein folding and unfolding are usually performed at pressures below 7 kbar, but some proteins need still higher pressures to unfold. The pressures needed to induce unfolding can be lowered by the application of chemical denaturants (like guanidinium hydrochloride or urea), as in studies of the trp repressor [11]. On the other hand, there are proteins that unfold at quite low pressures. Among them, there is the staphylococcal nuclease, which unfolds at a pressure of about 2 kbar [12].

The elevated pressure slows chemical reactions down (compared to the standard pressure) and it extends folding/unfolding times [13]. These features are notable, since elongation of kinetic timescales should facilitate experimental research on protein dynamics. At high pressures, proteins unfold within a very wide range of times, from seconds to even hours, which can be made shorter by working at elevated temperatures [14]. The description of the

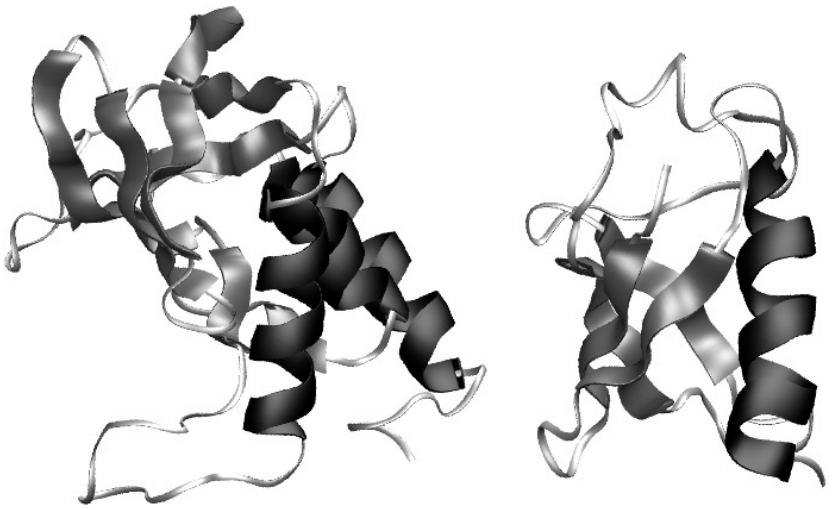

Figure 1. Structures of staphylococcal nuclease (1NUC, left) and ubiquitin (1V80, right) in a cartoon view. The α-helices are shown in the darker shade of grey. The figure was made in VMD [40].

combined effect of pressure, temperature and sometimes mutations [15] may be complicated. For instance, the unfolding time of the wild type (wt) staphylococcal nuclease increases with pressure, but at an elevated temperature, it first rises and then goes down [14]. However, mutated versions of staphylococcal nuclease may show the unfolding time that decreases with pressure [15]. This happens when one considers various mutations on the Val-66 residue in the so-called hyperstable form of staphylococcal nuclease (obtained from the wt through deletion of a loop, five residue long, and substitutions at five other sites).

In this paper, we focus on modelling of the effects of pressure in coarse-grained models. All-atom molecular dynamics simulations of proteins provide a detailed description of proteins. However, they are typically restricted to nanosecond timescales, which are inadequate in studies of processes involving large conformational changes. There is thus a need to develop coarse-grained molecular dynamics models that incorporate pressure-related effects. In this paper, we consider the Go-like approach [16] in which amino acids are represented by single effective beans located at the positions of the C^{α} atoms and the effective potentials between them are chosen phenomenologically, based on the native geometry of the protein under study. We discuss how these effective potentials need to be modified to include the influence of the pressure, and then we consider two specific examples of proteins: staphylococcal nuclease (snase) and ubiquitin. Both of these proteins have underwent studies in high-pressure experiments. Their native structures are shown in figure 1.

Snase is a protein that contains 149 amino acids and has no disulfide bonds. The radius of gyration, R_g, of the native structure of snase is about $\sim$17 Å. 26.2% of the structure is helices, 24.8% is β-sheets, 7.4% is extended chains, 24.8% is turns and loops, and 8.7% has no order. The onset of the pressure-induced denaturation of snase takes place at around 1.5 kbar. On increasing the pressure further to 3 kbar, there is a complete change in the structure: R_g grows to about 36 Å, the pair distribution function broadens up, and the contents of α helices and β sheets are lowered drastically [17, 18]. The large value of R_g, however, is smaller than 45 Å, which characterizes random coil conformations [19]. Furthermore, the observed relaxation times also grow with increasing pressure [13]. However, any changes introduced to

snase (mutations) or its environment (elevated temperature) cause changes in the behaviour of relaxation times [14, 15]. The relaxation processes are dominated by folding at pressures below 1.5 kbar and by unfolding at higher pressures.

Ubiquitin comprises 76 amino acids and also has no disulfide bonds. Its native structure contains five-strand mixed β-sheet, and a short α-helix. Ubiquitin changes its conformation slightly at 3 kbar, but it remains globular [20] until the pressure of 5.4 kbar, at which the denaturation starts to take place. The denaturation process gets completed at 6.4 kbar [21].

Experimental studies performed so far lead to the following insights: (a) proteins usually decrease their volume upon pressure-induced unfolding [22] and (b) the transition state between the folded and unfolded states corresponds to a high energy barrier [13]. The first of these observations indicates that the reduction in volume upon unfolding becomes more and more important with increasing pressure, and it drives equilibrium toward the unfolded state.

An insight that comes from theory is that pressure appears to affect the potentials of mean force (PMF) by building energy barriers atop Lennard-Jones-like intermolecular potentials, and by forming the second energy minimum beyond the barrier. The evidence for this effect follows from several studies dealing with the influence of pressure on hydrophobic model systems such as methane molecules placed in water [23–25]. The PMF derived for the methane molecules through molecular dynamics simulations indicates the emergence of a pressure-induced barrier that makes a distance between molecules of around 5–6 Å energetically unfavourable. This barrier grows with pressure and moves to shorter distances. In addition, the binding part of the potential is observed to become increasingly shallow, and the second energy minimum becomes deeper. The presence of the barrier is qualitatively related to the behaviour of the effective volume taken by two molecules when the distance between their centres varies. This effective volume is defined through the space that is inaccessible to water. When starting from the state of tight compression, this volume increases with the distance between the two molecules until one water molecule can fit between them; then it decreases and, eventually, reaches a saturation value, as illustrated schematically in figure 2. The rise in volume means an increase in the energy of the system in proportion to the pressure.

The kinetic processes in proteins are often described in terms of the two-state model, i.e. in terms of the folded, unfolded, and transition states. In pressure-induced unfolding, the volume variations in these states affect the free energies in a major way which, in addition, is likely to be specific to a protein. Thus we propose a model that is consistent with the behaviour of wt staphylococcal nuclease at room temperature.

The idea of including the pressure in simplified models by the introduction of an additional energy barrier, and the second minimum has been suggested before [26–29]. It has been implemented both in lattice [28] and continuous models at standard pressure [29]. The barrier generates an unfavourable region in hydrophobic interactions and thus eliminates conformations with large effective volumes. It then seems natural to implement such a barrier in Go-like models. The barrier could be operational in both binding native and repulsive non-native potentials. However, adding an extra hump to non-native contacts should result primarily in enlarging the effective size of the hard cores, which prevents entanglements. Thus the novel pressure-related phenomena should be due mostly to the native contacts.

We focus on the modelling of snase and ubiquitin around room temperature. The modification of the potential should be compatible with the experimental observations for wt staphylococcal nuclease, such as: (a) the processes of unfolding and folding become slower with pressure [13, 30] and (b) the folded state is preferred at atmospheric pressure and unfolded at higher pressures. The unfolding time of a protein at high pressure is very long—it may even reach several minutes. In order to make the studies accessible computationally, we consider barriers that are reduced in height and focus on qualitative features.

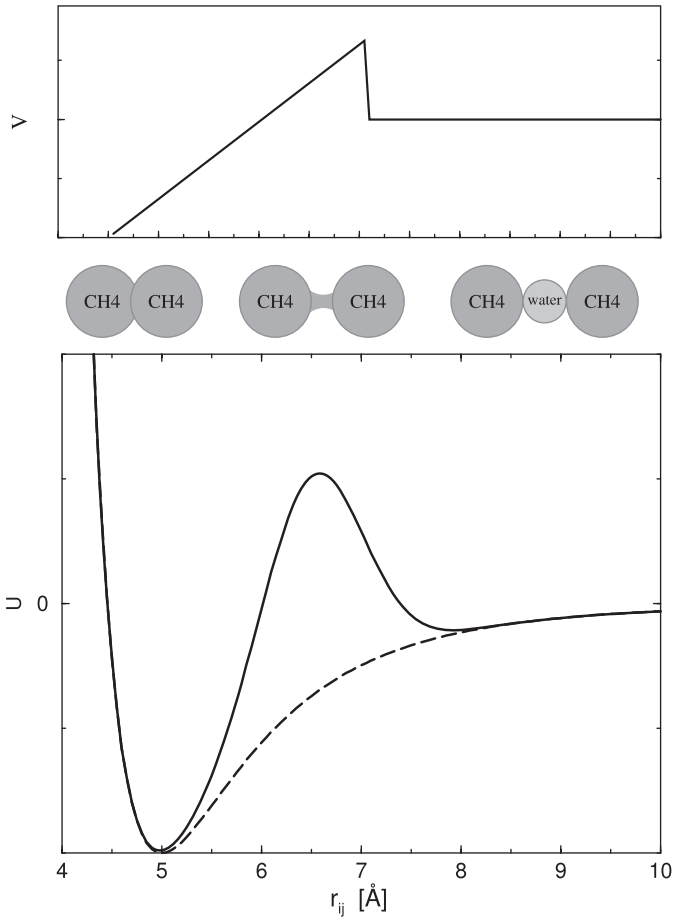

Figure 2. Top panel: the effective volume, V, increases with the distance between two nearby molecules of methane until at least one solvent molecule can fit between them. Afterwords, it drops and then stabilizes. Bottom panel: the solid line shows the expected form of the potential, U, between two amino acids in contact and in the presence of pressure. The dashed lines correspond to the $V_{\rm LJ}$ potential.

Our implementation of this phenomenological approach to staphylococcal nuclease is found to reproduce qualitatively the observed features in folding and unfolding kinetics and predicts the existence of a non-monotonic dependence of the relevant rates on pressure.

2. Methods

We base our approach on the version of the Go-like model that has been described in [31–34]. A protein is represented by a string of their C^{α} atoms that are tethered by harmonic springs:

$$V_{\rm tether} = \tfrac{1}{2}k(r_{i,i+1} - r^0_{i,i+1})^2, \tag{1}$$

where $r_{i,i+1}$ is the distance between two consecutive centres, and $r^0_{i,i+1}$ is the distance between these centres in the native structure. The elasticity constant, k, is taken to be 100 ϵ Å^{-2}. Additionally, to chain connectivity potentials, the local stiffness of the backbone is maintained

by chirality potentials,

$$V_{\text{chiral}} = \tfrac{1}{2}\epsilon \left(C_i - C_i^{\text{NAT}}\right)^2, \tag{2}$$

where $C_i = (\vec{v}_{i-1} \times \vec{v}_i) \cdot \vec{v}_{i+1}/d_o^3$, $\vec{v}_i = \vec{r}_{i+1} - \vec{r}_i$, and $d_0 = |v_i|$. One distinguishes between native and non-native interactions, or contacts, between the amino acids. The classification is based on the existence or absence of atomic overlaps in a way suggested by Tsai *et al* [35]. The native contacts between amino acids i and j are represented by the Lennard-Jones potential,

$$V_{\text{LJ}}(r) = 4\epsilon \left(\left(\frac{\sigma_{ij}}{r}\right)^{12} - \left(\frac{\sigma_{ij}}{r}\right)^{6} \right), \tag{3}$$

where ϵ is a uniform energy parameter and σ_{ij} is a length parameter that is selected so that the potential minimum corresponds to the native distance between the C^{α} s. The location of the minimum, r_{min}, is related to σ_{ij} through the equation $r_{\text{min}} = \sqrt[6]{2}\sigma_{ij}$. The non-native contacts are represented by the Lennard-Jones repulsive cores which are truncated at 4 Å. The time unit in the model, τ, in Lennard-Jones models of molecular systems is defined as $\sqrt{m\sigma/\epsilon}$, where m is the average mass of an amino acid and $\sigma = 5$ Å. It should be understood, however, that the model takes into account interactions with the implicit solvent in an effective, or renormalized, way and an agreement with experimental timescales is reached when τ is effectively of the order of nanoseconds. This is around 3 ns according to reference [36] or 0.25 ns according to hydrodynamics-related arguments of reference [37]. The molecular dynamics simulations involve solving Newton's equations of motion together with the Langevin noise that controls the temperature and provides damping. We use the damping constant $\gamma = 2m/\tau$ that produces the overdamped dynamics appropriate for proteins in a solvent [31]. That is roughly 25 times smaller than the damping from water, but our test for larger γ show a linear dependence of folding times with γ (in the case of a standard Go model without pressure).

In order to adjust this approach to pressure-related effects, it is convenient to begin by considering a potential in which the notions of the location of a minimum and of its width are divorced from each other. In the V_{LJ} potential, both quantities are controlled by a single parameter, σ_{ij}. In particular, a large value of r_{min} corresponds to a broad potential well. In this paper, instead we introduce an additional parameter s to control the width, independently of the location of a minimum, and the potential is given by

$$V_s(r) = 4\epsilon \left(\left(\frac{s}{r - \sqrt[6]{2}(\sigma_{ij} - s)}\right)^{12} - \left(\frac{s}{r - \sqrt[6]{2}(\sigma_{ij} - s)}\right)^{6} \right). \tag{4}$$

The parameter s is meant to be uniform—we take $\sqrt[6]{2}s = 5$ Å—whereas σ_{ij} is adjusted depending on the required location of the minimum. For $s = \sigma_{ij}$, $V_s(r)$ coincides with $V_{\text{LJ}}(r)$. Examples of V_s for $\sqrt[6]{2}s = 5$ Å and several values of σ_{ij} are shown in figure 3.

The presence of a constant width of the potential well with a minimum at r_{min} facilitates incorporation of the pressure-related barrier. We expect that the barrier should be small at atmospheric pressure, and should grow with pressure. The barrier, combined with V_s, should lead to the formation of a second minimum at a distance of $r_{\text{min}} + 3$ Å. The distance of 3 Å corresponds to the size of a water molecule, and the second minimum indicates the existence of a water-mediated attraction between two amino acids. The locations of the two minima should depend on the pressure, but the distance between them should stay approximately constant. Finally, the depth of the potential is expected to diminish with pressure. All of these conditions are satisfied by the potential V_{P}, which augments V_s by a

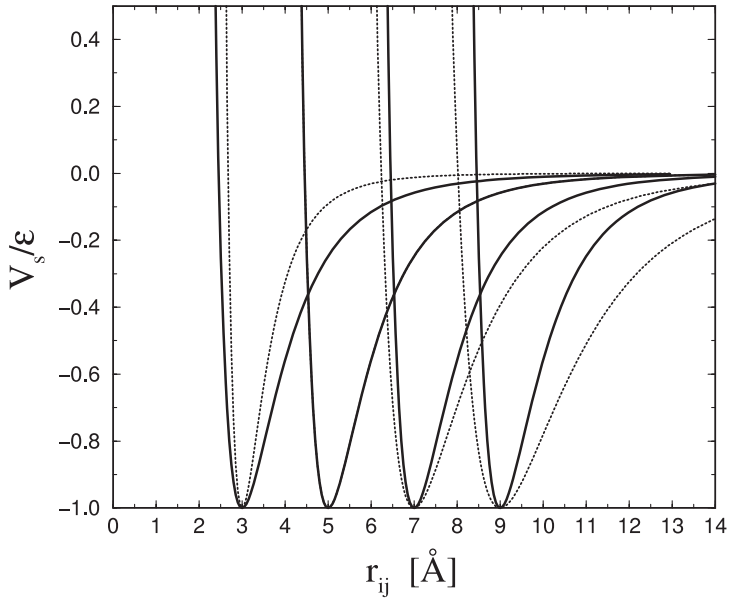

Figure 3. The dependence of the modified Lennard-Jones potential, V_s, (thick lines) and the standard Lennard-Jones potential (dotted lines) on r. The potentials are described by equation (4) with $\sqrt[6]{2}s = 5$ Å, and $\sqrt[6]{2}\sigma_{ij} = 3, 5, 7, 9$ Å (from left to right, respectively). For $\sqrt[6]{2}\sigma_{ij} = 5$ Å, both plots are the same.

hump term. It is defined as

$$V_{\mathrm{P}}(r) = \epsilon \left(4 \left(\left(\frac{s}{r - \sqrt[6]{2}(\sigma_{ij} - s)} \right)^{12} - \left(\frac{s}{r - \sqrt[6]{2}(\sigma_{ij} - s)} \right)^{6} \right) + A \cdot \mathrm{e}^{-(r-(\sqrt[6]{2}\sigma_{ij}+C))^2/B} \right), \tag{5}$$

where $\sqrt[6]{2s}$ is taken to be equal to 5 Å and A, B, and C are parameters that are controlled by pressure. Specifically, we take

$$\begin{aligned} A &= P + 0.3 \\ B &= -0.43\mathrm{e}^{-2.34A} + 0.77 \\ C &= 1.4\mathrm{e}^{-1.0A} + 0.7, \end{aligned} \tag{6}$$

where P is a dimensionless control parameter that is proportional to pressure. There are many possible parameters A, B and C. We chose them carefully to satisfy several assumptions on the resulting effective potential: (a) there must be two minima with a 3 Å gap between them; (b) at standard pressure, the first minimum should resemble the original Lennard-Jones potential; (c) the resulting simulations should give similar behaviour to that observed in experiments. Figure 4 shows examples of the potential V_{P} for several values of P. Note that the position of the first minimum keeps changing with increasing pressure more noticeably than that of the more distant minimum, but their separation remains around 3 Å. The properties of the system depend on the depth of the potential well and on the height of the barrier. If the well is sufficiently deep, folding is preferred over unfolding.

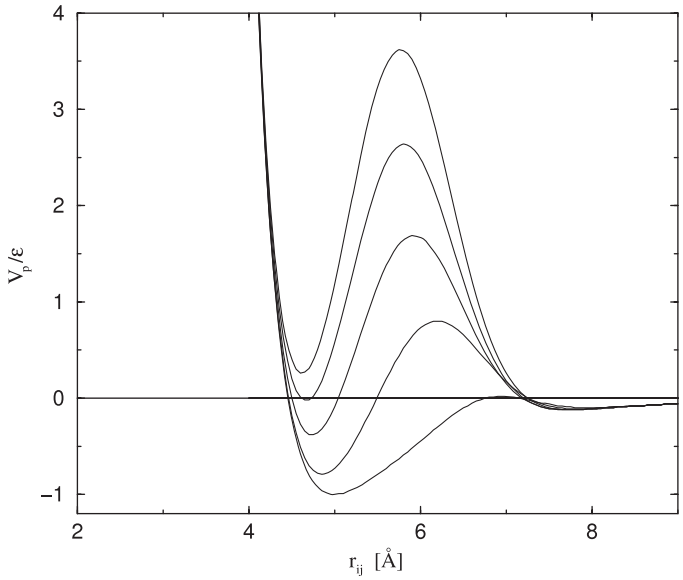

Figure 4. The dependence of the potential $V_{\rm P}$ on r for $s = 5$ Å and P equal to 0, 1, 2, 3, and 4 from the bottom to the top, respectively.

3. Results

We first consider the process of folding from an unfolded conformation. As the model protein folds, it establishes more and more contacts. In the Lennard-Jones-based model, a contact is considered to be established [31] when the distance between the corresponding C^α atoms becomes smaller than $1.5\sigma_{ij}$ (which is close to the inflection point in the potential [38]). Folding is considered to be accomplished when all of the native contacts are established simultaneously for the first time.

In the model with the P-dependent potential, the criterion for the existence of a contact has to be modified. A reasonable expectation is to say that a contact exists if the distance between the C^α atoms is smaller than the distance to the peak of the barrier. This situation corresponds to $r < r_c = r_{\rm min} + \Delta r$, where $r_{\rm min}$ is the distance between C^α atoms in their native conformation and Δr is the distance between $r_{\rm min}$ and the top of the hump. Since the position of the hump changes with pressure, Δr should also be a function of P. Approximately, $\Delta r = 1.5{\rm e}^{-0.9A} + 0.75$ (Å) (where A is defined in equation (6)).

The hump sets up a penalty for breaking the contact, and its height determines the timescale of the process. The interpretation of the second minimum is not straightforward. It might seem that the second minimum corresponds to residue–residue interactions that are mediated by one water molecule. However, water molecules may enter available space only at the surface of a protein and not in buried regions. Thus hydratation levels cannot be determined simply by counting the contacts established in the secondary minima, as assumed in [29].

Figure 5 compares the dependence of the median folding time on temperature between two models: with the Lennard-Jones potentials and with the P-dependent potentials for different pressures, P. The folding times in the latter model are expected to be longer because of two factors: the presence of the barrier and a tighter criterion for contact establishment. The presence of the barrier should also move the temperature of optimal folding to higher values.

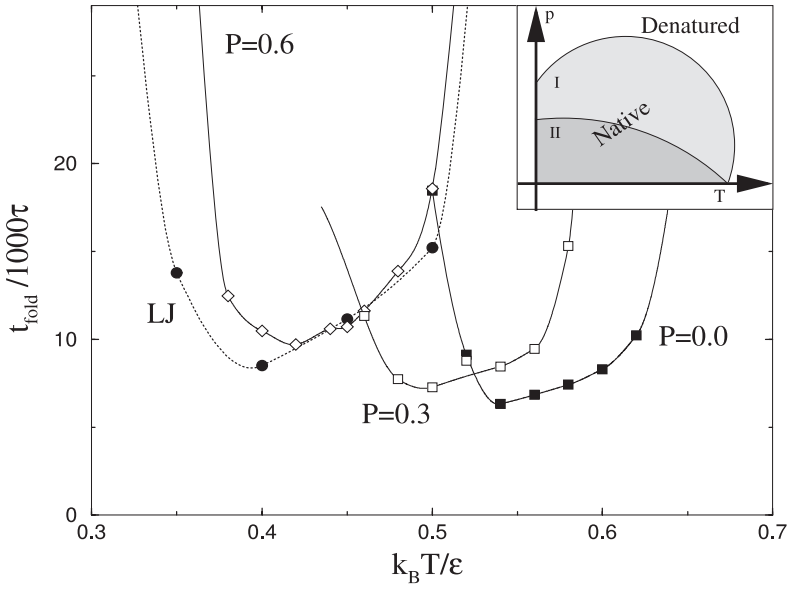

Figure 5. The dependence of the median folding times on temperature for snase. The solid lines represent results obtained in the P-dependent model for different values of P ($P = 0.0$, filled squares; $P = 0.3$, empty squares; $P = 0.6$, empty diamonds). The dotted line and circles correspond to the standard Lennard-Jones potential. The results are based on 101 trajectories. The inset shows a schematic representation of the P–T diagrams for proteins, as proposed by Smeller [6].

Generally, the latter expectation is fulfilled—with the temperature of optimality shifting from 0.4 to 0.55 k_BT/ϵ. Surprisingly, however, the folding times near the optimal conditions are actually slightly lower in the model that incorporates the pressure-related barrier than in the Lennard-Jones-based model. This effect is presumably due to a more precise locking of the contacts into place if the temperature allows for an adequate diffusion across conformations. For higher values of P (but still for pressures that keep protein in the folding state) folding times increase a little. This is reasonable, since the height of the barrier that the system has to pass gets bigger, so the expected times of diffusion should also become larger. However, the region of optimal folding moves toward lower temperatures, which seems unexpected. This behaviour is consistent with the the phase diagram shown in the inset of figure 5. The reason is that, for higher pressures, proteins became less stable, due to shallower potential wells, resulting in lower temperatures of denaturation.

The dependence of the folding times on temperature for different values of P, looks interesting. It is consistent with experimental and theoretical studies which predict an elliptical region of stability [6] when plotted on the P–T phase diagram (as shown in the inset of figure 5). The proteins could behave according to either scheme I or scheme II. According to scheme I, as the pressure grows, the protein may became more stable at the beginning, but a further pressure increase leads to destabilization and unfolding. According to scheme II, the protein becomes less stable with the increasing pressure, and it unfolds eventually. However, it is too early to state that simulations of snase in our model behave according to scheme I or II. Within our coarse-grained model, the explanation for the elliptical shape is easy. At standard pressure, the potential for native contacts is fixed—it has one major minimum, with the depth of ϵ, and a barrier of some height. As the pressure grows, the position and depth

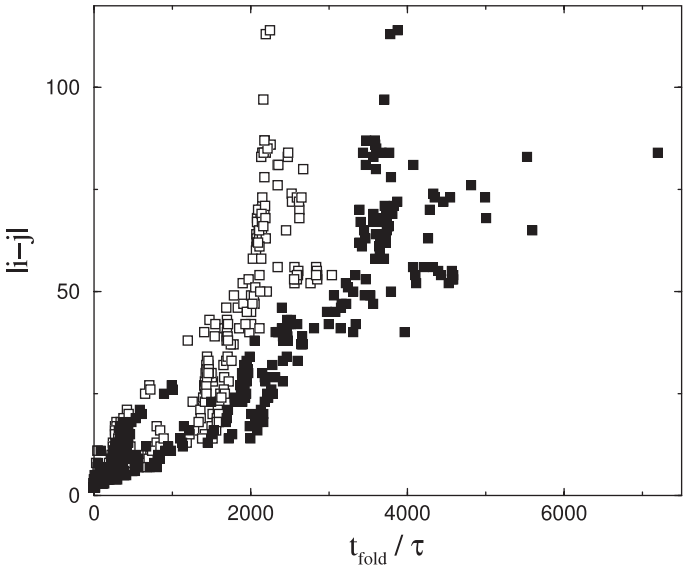

Figure 6. The folding scenarios for snase at the respective optimal temperatures in the standard model (open squares; at $k_B T = 0.4\epsilon$) and the P-dependent model (solid squares; at $k_B T = 0.55\epsilon$). It should be noted that the median folding time for the protein in the P-dependent model at $k_B T = 0.55\epsilon$ is 6592τ (figure 5), whereas the average time of forming the last contact is 7194τ. This might seem odd, but it is merely a result of considering quantities that are defined differently in the statistical ensemble of the trajectories.

of the minimum change, and the barrier height gets enhanced. These factors act in opposite ways, e.g. an increase in the barrier height stabilizes the folded structure, but an increase in the potential minimum destabilizes the structure. Either of the two P–T schemes may then result, depending on which of the two factors wins and this, in turn, may depend on the protein. Whatever the scheme, very high pressures lead to denaturation.

One can get insights into the details of folding by presenting the so-called folding scenarios [31] in which one shows the average times of establishing a contact for the first time during the folding process. In these diagrams, the contact is identified by its sequential distance $|i - j|$. Figure 6 indicates that, at its optimal temperature, individual contacts in the standard model are established sooner than in the P-dependent model. Thus the presence of barriers stretches the initial stages of the process. The final native state is reached sooner, however, since the system is more likely not to open contacts once they are established.

We now focus on the pressure-induced unfolding from the native state. We study this process at the temperature of optimal folding. The simultaneous breakage of all contacts at this temperature is hard to attain in simulations (for a further discussion, see reference [39]). We thus divide the contacts into two groups—local, with $|i - j| \leqslant 4$, and non-local—and consider unfolding to be realized when all non-local contacts are broken. The non-local contacts constitute about 60% of all contacts in our model. The dependence of the resulting unfolding times, t_{unfold}, on P is shown in figure 7. The figure suggests that t_{unfold} first decreases with an increasing P, then reaches a region of optimality (for $1.5 < P < 2.5$) and then rises again. This behaviour suggests that the application of pressure readily initiates unfolding, but the experimentally observed [13] extension of t_{unfold} should occur only at sufficiently high pressures. The threshold for the extension depends on the parameters describing the hump in

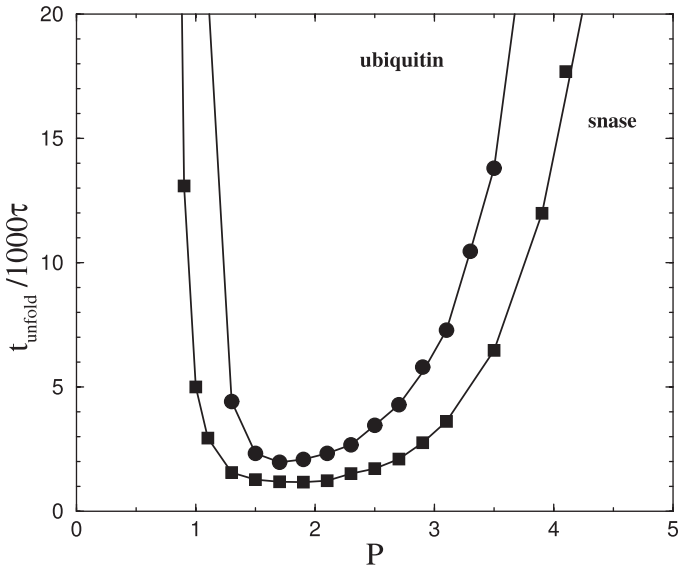

Figure 7. Dependence of the median unfolding time on the parameter P. The simulation temperature was set to be $0.55k_BT/\epsilon$ for snase, and $0.45k_BT/\epsilon$ for ubiquitin. The data points are based on 101 trajectories.

the potential. Comparison of the unfolding graphs for snase and ubiquitin (figure 7) shows that ubiquitin is more stable at high pressure than snase (the process of unfolding starts at $P = 1.3$ for ubiquitin and at $P = 1.0$ for snase). This feature agrees with experiments qualitatively, since snase starts to unfold at 1.5 kbar and ubiquitin at 3 kbar.

Another way to characterize the unfolding process is to study the behaviour of the quantity Q, defined as the fraction of the established native contacts, as a function of time. This is shown in figure 8 for several values of P. The results average to smooth exponential functions for P larger than 1.6 and then the functions $Q(t)$ look similar to the relaxation profiles obtained by Vidugiris *et al* [13]. It is seen that the characteristic times obtained in this way follow the behaviour of $t_{\rm unfold}$ shown in figure 7.

Both high pressure and high temperature can denaturate proteins, but the two processes are distinct. The snase protein consists of several secondary structures; see table 1. While the local contacts arise and break continuously, the non-local contacts show a structure in the scenario diagrams. Figure 9 shows that the scenario diagrams for the non-local contacts are different for the two kinds of unfolding processes. In thermal unfolding, the long-range contacts break the first and the dependence on $|j - i|$ is mostly monotonic. For the pressure-induced unfolding, shown for $P = 3.5$, the scenario is more complicated and with more pronounced time gaps between various groups of events.

Figure 10 shows the order of unraveling of the native structure of snase by marking the secondary structures by shades that indicate the time of unraveling them. The main difference between the temperature and pressure-induced unfolding is stronger stabilization of the helical region of protein in the latter. In the thermal process, the last breaking contacts were located in the core of the protein, and contacts that lie at the surface of the protein were broken the first. For the pressure-induced unfolding, one could observe similar behaviour, but an extended stability of the helices is distinct.

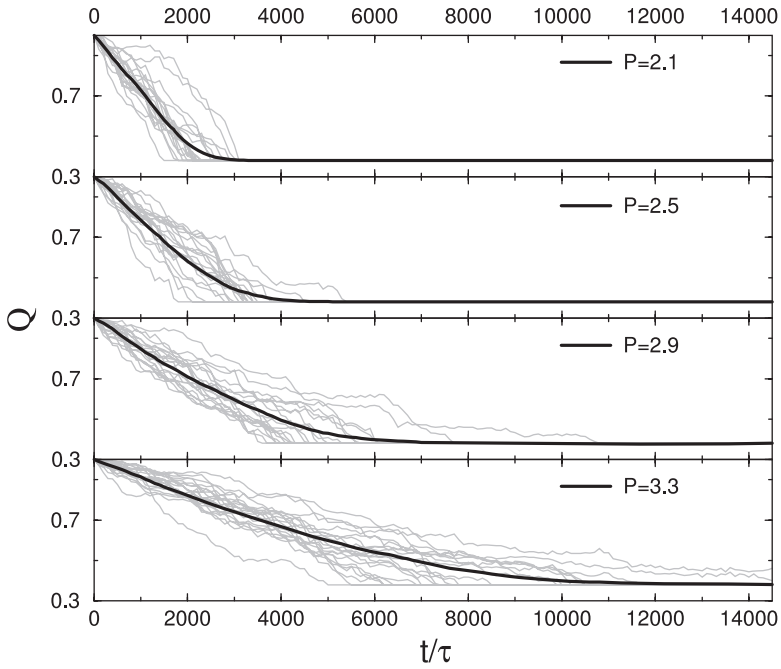

Figure 8. Fraction of the native contacts as a function of time during unfolding from the native state at selected values of the parameter P. The solid line shows an average over 101 trajectories, whereas the thin lines correspond to examples of individual trajectories.

Table 1. Secondary structures in snase. Each structure has a name that is listed in the last column.

Sequence	Structure	Name
Gly 55–Glu 67	Helix	A
Val 99–Gln 106	Helix	B
Glu 122–Lys 134	Helix	C
Lys 9–Ala 12	Strand	D
Ile 72–Phe 76	Strand	E
Gly 88–Ala 94	Strand	F
Gln 30–Leu 36	Strand	G
Thr 22–Tyr 27	Strand	H
Thr 13–Ala 17	Strand	I
Val 39–Thr 41	Strand	J
Ala 109–Val 111	Strand	K

One way to characterize the effects of pressure is to provide average displacement distances, Δr, of the C^{α} atoms in structures arising at the elevated pressure, relative to the native structure at the standard pressure. Figure 11 compares Δr as obtained in an experimental nuclear magnetic resonance (NMR) study of ubiquitin by Kitahara [20] to the one obtained theoretically within our model. We observe qualitative agreement of the theoretical modelling with the experimental findings, except near the N terminal. (The procedure for determining Δr is outlined in the caption, and it involves overlapping the dynamically obtained structures with the native structure. Such a procedure is less reliable when it comes to the near-terminal

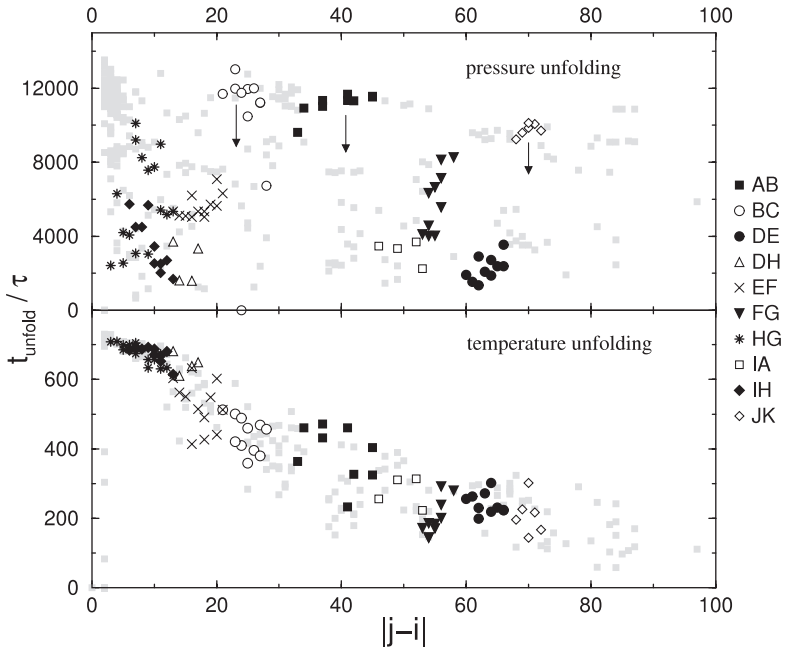

Figure 9. The unfolding scenario for snase as induced by temperature (for $k_B T/\epsilon = 1.0$, $P = 0.0$, the bottom panel) and by high pressure (for $k_B T/\epsilon = 0.5$, $P = 3.5$, the top panel). The duration of contacts is presented as a function of the sequential distance $|j - i|$, or contact order, for the contacts. Different shapes of the points describe contacts between different secondary structures, e.g. contact AB means all contacts between structure A and structure B (see table 1 for the sequential assignment of the secondary structures). The temperature induced unfolding has a clear pattern of contact breaking: the contact with a large order break earlier than those with the small contact order. The pressure induced unfolding scenario could be divided into three zones: (I) contacts that break similar to the temperature unfolding process: e.g. DE (filled circles), AI (empty squares), EF (cross); (II) contacts that break sooner than in I: DH (empty triangles), HG (stars), IH (filled diamonds); (III) contacts that break later than in I: AB (filled squares), BC (empty circle), JK (empty diamonds). The arrows describe major changes in the scenario at lower pressures, three structure contacts lower their times of breaking, but still remain in area of the late breaking times.

regions.) The most significant changes are located between helix 22–35 and β-strand 42–46 and then in other segments which either lack secondary structures or correspond to turns. The reason for this behaviour is that helices and sheets contain more contacts and are thus more stable. All of the substantially affected regions are located in space just near the C-terminus.

In summary, we have demonstrated that the experimentally known effects of pressure can be described by a simple coarse-grained geometry-based model by adding a pressure-controlled hump in the effective potential. We have shown that the unfolding times can be non-monotonic functions of pressure and have a region of optimality. Our model does not address non-pressure-related changes in the volume of the protein. The pressure-induced and temperature-induced unfolding processes proceed differently. This observation, however, is made for snase only, and could not yet be generalized for all proteins. The simulations for ubiquitin shows that ubiquitin is stable in a wider range of pressures than snase, and it agrees with experimental observations for the wild-type snase around room temperature. The results of simulations of ubiquitin at elevated pressure are also consistent with the NMR studies.

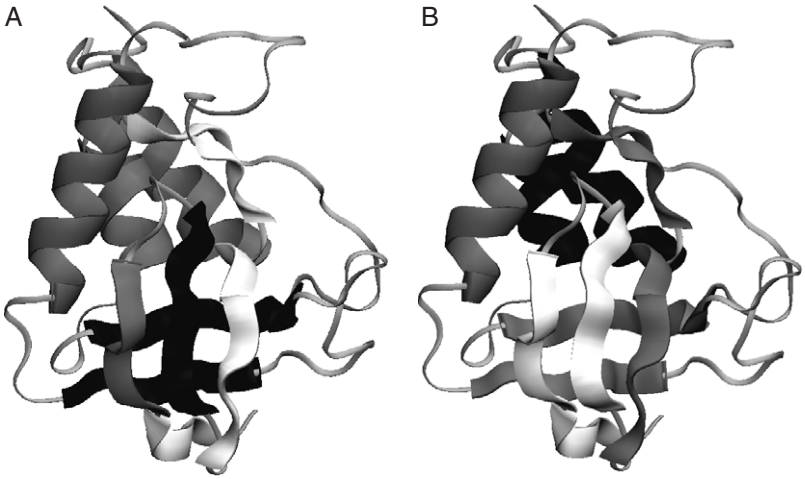

Figure 10. The native structure of snase shaded according to the time at which contacts between specific secondary structures are broken. The A and B panels are for the temperature and pressure induced unfolding respectively. The white, grey, and black shapes correspond to the early, middle, and late periods of unfolding respectively. For the thermal unfolding, the core of the protein is affected in the late period, the helices are affected in the middle period, and the β strands on the surface of the protein are broken in the beginning. For the pressure-induced unfolding, the helices break the last, the core in the middle period, and the β strands on the surface of the protein at the beginning. Figure was made in VMD [40].

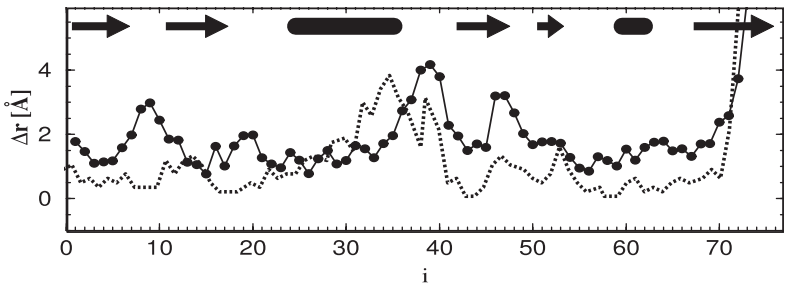

Figure 11. The average displacement of the C^{α} atoms in ubiquitin relative to the native structure for a given sequential position i. The dotted line presents results from the experimental study of Kitahara [20]. The continuous line and filled circles were obtained theoretically at $P = 0.2$ and $k_B T = 0.4\epsilon$. The reference structure, at standard pressure, is represented by the first structure in the 1V80.pdb file in the PDB. Ten trajectories of duration $100\,000\tau$ were considered. 100 structures were selected and then overlapped on the template structure to determine the displacement. The procedure of overlapping made use of the program and the server of Zemla [41]. Helices and β-structures are depicted by thick lines and arrows, respectively, at the top of the graph.

Acknowledgment

This work was funded by the Ministry of Science in Poland (grant 2P03B 03225).

References

[1] Li T M, Hook J W III, Drickamer H G and Weber G 1976 *Biochemistry* **15** 3205
[2] Weber G and Drickamer H G 1983 *Q. Rev. Biophys.* **16** 89

[3] Markley J L, Northrop D B and Royer C A (ed) 1996 *High Pressure Effects in Molecular Biophysics and Enzymology* (Oxford: Oxford University Press)
[4] Jonas J 2002 *Biochim. Biophys. Acta* **1595** 145
[5] Doster W and Gebhardt R 2003 *Chem. Phys.* **292** 383
[6] Smeller L 2002 *Biochim. Biophys. Acta* **1595** 11
[7] Bridgeman P 1914 *J. Biol. Chem.* **19** 511
[8] Mozhaev V, Heremans K, Frank J, Masson P and Balny C 1996 *Proteins* **24** 81
[9] Silva J and Weber G 1993 *Annu. Rev. Phys. Chem.* **44** 89
[10] Tan C, Xu C and Ruan K 2006 *Biochim. Biophys. Acta* **1764** 481
[11] Desai G, Panick G, Zein M, Winter R and Royer C 1999 *J. Mol. Biol.* **288** 461
[12] Royer C, Hinck A, Loh S, Prehoda K, Peng X, Jonas J and Markley J 1993 *Biochemistry* **32** 5222
[13] Vidugiris G J A, Markley J L and Royer C A 1995 *Biochemistry* **34** 4909
[14] Panick G, Vidugiris G, Malessa R, Rapp G, Winter R and Royer C 1999 *Biochemistry* **38** 4157
[15] Brun L, Isom D, Velu P, Garcia-Moreno B and Royer C 2006 *Biochemistry* **45** 3473
[16] Go N and Abe H 1981 *Biopolymers* **20** 991
[17] Panick G, Malessa R, Winter R, Rapp G, Frye K J and Royer C A 1998 *J. Mol. Biol.* **275** 389
[18] Paliwal A, Asthagiri D, Bossev D P and Paulaitis M E 2004 *Biophys. J.* **87** 3479
[19] Miller W G and Goebel C V 1968 *Biochemistry* **7** 3925
[20] Kitahara R, Yokoyama S and Akasaka K 2005 *J. Mol. Biol.* **347** 277
[21] Herberhold H and Winter R 2002 *Biochemistry* **41** 2396
[22] Royer C A 2002 *Biochim. Biophys. Acta* **1595** 201
[23] Ghosh T, Garcia A E and Garde S 2002 *J. Chem. Phys.* **116** 2480
[24] Ghosh T, Garcia A E and Garde S 2001 *J. Am. Chem. Soc.* **123** 10997
[25] Ghosh T, Garcia A E and Garde S 2003 *J. Phys. Chem.* B **107** 612
[26] Onuchic J N, Nymeyer H, Garcia A E, Chahine J and Socci N D 2000 *Adv. Protein Chem.* **53** 87
[27] Hummer G, Garde S, Garcia A, Paulatis M and Pratt L 1998 *Proc. Natl Acad. Sci. USA* **95** 1552
[28] Hillson N, Onuchic J N and Garcia A E 1999 *Proc. Natl Acad. Sci. USA* **96** 14848
[29] Cheung M S, Garcia A E and Onuchic J N 2002 *Proc. Natl Acad. Sci. USA* **99** 685
[30] Wagner G 1980 *FEBS Lett.* **112** 280
[31] Cieplak M and Hoang T X 2003 *Biophys. J.* **84** 475
[32] Cieplak M, Hoang T X and Robbins M O 2004 *Proteins Struct. Funct. Biol.* **56** 285
[33] Baker D 2000 *Nature* **405** 39
[34] Micheletti C, Banavar J R and Maritan A 2001 *Phys. Rev. Lett.* **87** 088102
[35] Tsai J, Taylor R, Chothia C and Gerstein M 1999 *J. Mol. Biol.* **290** 253
[36] Veitshans T, Klimov D and Thirumalai D 1997 *Folding Des.* **2** 1
[37] Szymczak P and Cieplak M 2006 *J. Chem. Phys.* **125** 164903
[38] Kwiecinska J I and Cieplak M 2005 *J. Phys.: Condens. Matter* **17** S1565
[39] Cieplak M and Sulkowska J I 2005 *J. Chem. Phys.* **123** 194908
[40] Humphrey W, Dalke A and Schulten K 1996 *J. Mol. Graph* **14** 33
[41] Zemla A 2003 *Nucleic Acids Res.* **31** 3370